# Predicting the ground-state structure of sodium boride

Xin-Ling He, Xiao Dong, QuanSheng Wu, Zhisheng Zhao, Qiang Zhu, Artem R. Oganov,

Yongjun Tian, Dongli Yu, Xiang-Feng Zhou, and Hui-Tian Wang

# Predicting the Ground State Structure of Sodium Boride

Xin-Ling He,[1] Xiao Dong,[1] QuanSheng Wu,[2] Zhisheng Zhao,[3] Qiang Zhu,[4] Artem R. Oganov,[5, 6, 7] Yongjun Tian,[3] Dongli Yu,[3] Xiang-Feng Zhou,[1, *] and Hui-Tian Wang[1, 8]

[1] *Key Laboratory of Weak-Light Nonlinear Photonics and School of Physics, Nankai University, Tianjin 300071, China*

[2] *Institute of Physics, ÉcolePolytechniqueFédérale de Lausanne (EPFL), CH-1015 Lausanne, Switzerland*

[3] *State Key Laboratory of Metastable Materials Science and Technology,*
*Yanshan University, Qinhuangdao 066004, China*

[4] *Department of Physics and Astronomy, High Pressure Science and Engineering Center,*
*University of Nevada, Las Vegas, NV 89154, USA*

[5] *Skolkovo Institute of Science and Technology, 3 Nobel St., Moscow 143026, Russia*

[6] *Moscow Institute of Physics and Technology, Dolgoprudny, Moscow Region 141700, Russia*

[7] *Department of Geosciences, Center for Materials by Design,*
*and Institute for Advanced Computational Science,*
*Stony Brook University, Stony Brook, New York 11794, USA*

[8] *National Laboratory of Solid State Microstructures and Collaborative Innovation*
*Center of Advanced Microstructures, Nanjing University, Nanjing 210093, China*

Binary borides had been a subject of extensive research. However, the exact compositions and crystal structures of sodium borides remained controversial. Here, using the *ab initio* variable-composition evolutionary algorithm, a new stable $Na_2B_{30}$ with $I2_12_12_1$ symmetry ($I2_12_12_1$-$Na_2B_{30}$) is found, which is -7.38 meV/atom lower in energy than the experimental $Imma$-$Na_2B_{30}$ structure. Interestingly, the $Imma$-$Na_2B_{30}$ is predicted to be a topological nodal line semimetal, which may result in superior electronic transport. In contrast, $I2_12_12_1$-$Na_2B_{30}$ is an ultrahard semiconductor with an unprecedented open-framework structure, whose interstitial helical boron sublattice enhances its hardness and energetic stability.

The discovery of high-temperature superconductivity, superhardness, ferromagnetism and quantum topological properties in metal borides has attracted much attention owing to many interesting fundamental issues and huge potential applications.[1–6] For alkali metal borides, only a few compounds have been precisely determined with regard to their compositions and structures. This is mainly limited by the synthesis and characterization of these materials, e.g., it is difficult to conduct a controlled reaction between the low-melting alkali metals with boron under ambient pressure, and products are often microcrystalline powders, rather than single crystals.[7–10] So far, there are only two sodium borides, orthorhombic $Na_3B_{20}$ and $Na_2B_{30}$ (or monoclinic $Na_2B_{29}$), which were successfully synthesized at ambient pressure.[7–9] However, the exact structure and composition of "$Imma$-$Na_2B_{30}$" are still controversial. Previously, Naslain and Kasper refined the structure as orthorhombic $Na_2B_{30}$ (designated as $\phi$ phase). This structure consists principally of $B_{12}$ icosahedra with interstitial boron triangular units, in which Na atoms are accommodated in the cages formed by icosahedra.[7] Since the unit cell of $Na_3B_{20}$ contains four formula units, it could be written as $4*NaB_3B_{12}$. However, by using X-ray diffraction (XRD), neutron diffraction, electron microscopy and solid-state NMR spectroscopy, Albert *et al* revised the structure as monoclinic $Na_2B_{29}$ ($2*NaB_3B_{12}+2*NaB_2B_{12}$) with two of interstitial B atoms per unit cell unoccupied ($Cm$-$Na_2B_{29}$).[8] To study the controversy, we performed *ab initio* calculations for the two structural models and found

that: (1) the relaxed $Na_2B_{29}$ had orthorhombic symmetry ($Imm2$-$Na_2B_{29}$), which is inconsistent with the reported monoclinic symmetry;[8] (2) $Imma$-$Na_2B_{30}$ is energetically more favorable than $Imm2$-$Na_2B_{29}$ in the Na-B system; (3) The band structure shows that $Imma$-$Na_2B_{30}$ is a topological nodal line semimetal, rather than a metal.[11] These intriguing results inspire us to further explore the polymorphism, phase diagram, and properties of this important compound.

To find stable Na-B compounds and structures, we utilized the *ab initio* evolutionary algorithm USPEX[12] allowing up to 40 atoms per primitive cell, and searching for all stable stoichiometries and their corresponding structures simultaneously. A phase is deemed stable if its enthalpy of formation from either elements or any other possible compounds is negative, and such method has been successfully applied to various bulk systems.[13–16] Structure relaxations and total energy calculations used the all-electron-projector-augmented wave[17] (PAW) method as implemented in the VASP package[18] with $[1s^2]$ cores for each Na and B atoms, the exchange-correlation energy was treated within the generalized gradient approximation (GGA), using the functional of Perdew, Burke, and Ernzerhof (PBE).[19] In addition, the local density approximation (LDA) with the functional of Ceperley and Alder,[20] as parametrized by Perdew and Zunger,[21] was also employed to confirm the energetic stability. The plane-wave cutoff energy of 500 eV and uniform $\Gamma$-centered $k$-points grids with the resolution of $2\pi \times 0.04$ Å$^{-1}$ were used. Denser $k$-
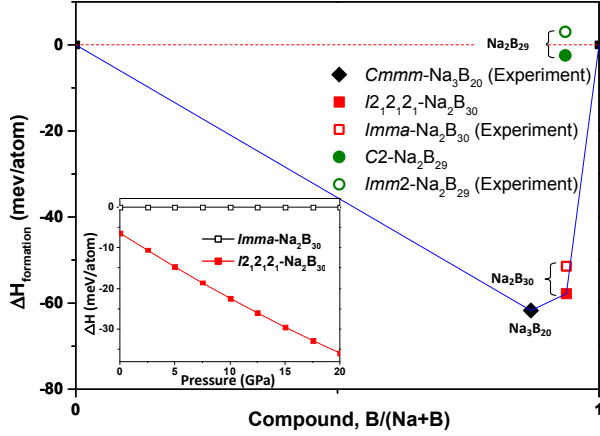
FIG. 1. The calculated convex hull for the Na-B system, using $bcc$-Na and $\alpha$-boron structures for pure elements. Here, $\Delta \mathrm{H}_{formation}(\mathrm{Na}_x\mathrm{B}_{1-x}) = \mathrm{H}(\mathrm{Na}_x\mathrm{B}_{1-x})-x\mathrm{H}(\mathrm{Na})-(1-x)\mathrm{H}(\mathrm{B})$. The inset shows the enthalpy difference between $Imma$-$\mathrm{Na}_2\mathrm{B}_{30}$ and $I2_12_12_1$-$\mathrm{Na}_2\mathrm{B}_{30}$ as a function of pressure.



FIG. 2. Structures of $Imma$-$\mathrm{Na}_2\mathrm{B}_{30}$ and $I2_12_12_1$-$\mathrm{Na}_2\mathrm{B}_{30}$. (a) Projection of $Imma$-$\mathrm{Na}_2\mathrm{B}_{30}$ along [100] direction. (b) Projection of $Imma$-$\mathrm{Na}_2\mathrm{B}_{30}$ along [010] direction. (c) Projection of $I2_12_12_1$-$\mathrm{Na}_2\mathrm{B}_{30}$ along [100] direction. (d) Projection of $I2_12_12_1$-$\mathrm{Na}_2\mathrm{B}_{30}$ along [010] direction. The Na and B atoms are colored in purple and brown, and the interstitial B atoms in the two structures are magnified for clarity.

points grids were tested, but produced indistinguishable results. The convergence for terminating the electronic self-consisting cycle and the force criterion for structure relaxation were set to $10^{-6}$ eV and $10^{-2}$ eV/Å, respectively. The phonon dispersion curves were calculated using the finite displacement method as implemented in the PHONOPY package,[22] where the precision convergence criteria for the total energy was $10^{-6}$ eV. Elastic tensors were computed by stress-strain relations. Combined with Voigt-Reuss-Hill approximation,[23] the bulk and shear moduli were calculated by CASTEP code at the GGA-PBE level.[24] Powder XRD patterns were simulated using the REFLEX software. Topological properties were investigated by constructing maximally localized Wannier functions[25] using WannierTools code.[26]

The convex hull plotted in Fig. 1 showed two stable compounds at ambient pressure. One can see that there are indeed only two stable stoichiometries, $\mathrm{Na}_3\mathrm{B}_{20}$ and $\mathrm{Na}_2\mathrm{B}_{30}$, consistent with the available experimental reports. Especially, the predicted lattice constants and atomic position of the $\mathrm{Na}_3\mathrm{B}_{20}$ are in excellent agreement with the experimental values.[9] This illustrates the power, reliability and accuracy of the USPEX method. However, the experimental $Imm2$-$\mathrm{Na}_2\mathrm{B}_{29}$ structure has a positive formation energy (3.03 meV/atom), and is far from the convex hull. Additionally, structure search also found a new monoclinic $\mathrm{Na}_2\mathrm{B}_{29}$ ($C2$-$\mathrm{Na}_2\mathrm{B}_{29}$), which had lower formation energy (-2.45 meV/atom) than $Imm2$-$\mathrm{Na}_2\mathrm{B}_{29}$, but still above the convex hull formed by $\mathrm{Na}_3\mathrm{B}_{20}$ and $\mathrm{Na}_2\mathrm{B}_{30}$, indicating that both structures of $\mathrm{Na}_2\mathrm{B}_{29}$ are at most metastable phases. Unexpectedly, it was not the much-discussed $Imma$-$\mathrm{Na}_2\mathrm{B}_{30}$, but a new polymorph $I2_12_12_1$-$\mathrm{Na}_2\mathrm{B}_{30}$ that appeared on the convex hull, and therefore predicted to be one of the true ground-state phases in the Na-B system, because it has lower en-
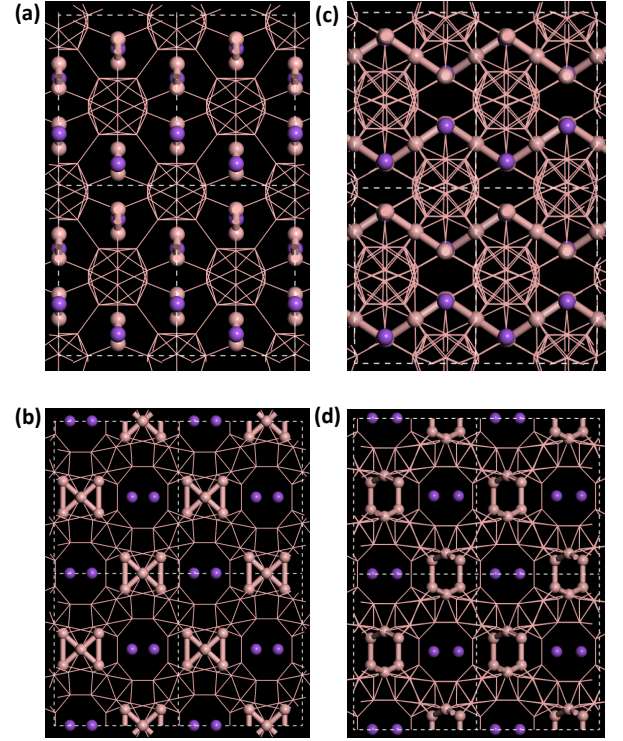
thalpy than the mixture of elemental Na and B, or any other mixtures. As shown in Table 1, the GGA-PBE results show that $I2_12_12_1$-$\mathrm{Na}_2\mathrm{B}_{30}$ is -6.37 meV/atom and -60.84 meV/atom lower in formation energy than the $Imma$-$\mathrm{Na}_2\mathrm{B}_{30}$ and $Imm2$-$\mathrm{Na}_2\mathrm{B}_{29}$ structures. The LDA calculations show the corresponding values are -18.14 meV/atom and -77.34 meV/atom accordingly, i.e., both GGA-PBE and LDA give the same ranking of structures by stability. Inclusion of zero point energy from GGA-PBE results only was strengthening our conclusion: $I2_12_12_1$-$\mathrm{Na}_2\mathrm{B}_{30}$ is now more stable than $Imma$-$\mathrm{Na}_2\mathrm{B}_{30}$ by -7.38 meV/atom. Moreover, the enthalpy difference (as a function of pressure; see the inset of Fig. 1) confirm that $I2_12_12_1$-$\mathrm{Na}_2\mathrm{B}_{30}$ is more stable than $Imma$-$\mathrm{Na}_2\mathrm{B}_{30}$ at any pressure.

These two crystal structures are compared in Fig. 2. For the $Imma$-$\mathrm{Na}_2\mathrm{B}_{30}$ structure, the Na atom sits at Na (0.000 0.250 0.089), six inequivalent B atoms occupy sites B1 (0.202 0.089 0.915), B2 (0.169 0.002 0.713), B3 (0.395 0.250 0.144), B4 (0.649 0.250 0.903), B5 (0.000 0.250 0.497), and B6 (0.915 0.250 0.796). Among them, Na, B3, and B5 are interstitial atoms, i.e., not belonging to any $\mathrm{B}_{12}$-icosahedra. The icosahedra are connected either

by direct inter-icosahedral B-B bonds (two-electron-two-center bonds with the lengths of 1.766 Å and 1.755 Å) or by three-center bonds with bond lengths of 2.078 Å and 1.746 Å (see Figs. 2a and 2b). The $Imm2$-$Na_2B_{29}$ structure, as mentioned above, is just a modified version of $Imma$-$Na_2B_{30}$, obtained by removing two interstitial B atoms from their interstitial triangular boron units in the unit cell, resulting in 3.33% boron vacancy concentration. On the other hand, atomic positions in the $I2_12_12_1$-$Na_2B_{30}$ structure are completely different from those of $Imma$-$Na_2B_{30}$ (see Figs. 2c and 2d): Na (0.000 0.250 0.149), eight inequivalent B atoms occupy sites B1 (0.587 0.741 0.363), B2 (0.332 0.996 0.039), B3 (0.171 0.478 0.953), B4 (0.191 0.095 0.337), B5 (0.917 0.238 0.469), B6 (0.189 0.419 0.339), B7 (0.840 0.232 0.663), and B8 (0.368 0.000 0.250). Among them, the interstitial B1 and B8 atoms form a peculiar helical sublattice, which link $B_{12}$-icosahedra by multicenter B-B-B bonds with varied bond lengths ranging from 1.711 to 2.058 Å.

Table 1 compares calculated properties of various models of $Na_2B_{30}$ and $Na_2B_{29}$ with experimental values. All three models have similar lattice constants and densities (compare lattice parameters of $I2_12_12_1$-$Na_2B_{30}$ with the experimental values,[7,8] the maximum difference in lattice parameters a, b, and c are 1.16%, 2.56%, and 2.25%), and all three are in good agreement with experimental results. It is unsurprising that $Imma$-$Na_2B_{30}$ and $Imm2$-$Na_2B_{29}$ have similar lattice constants because they are just two versions of the same structure, while $I2_12_12_1$-$Na_2B_{30}$ has a completely different structural topology. Therefore, we simulated the X-ray diffraction patterns of the $Imm2$-$Na_2B_{29}$, $Imma$-$Na_2B_{30}$, and $I2_12_12_1$-$Na_2B_{30}$ structures, and compared them with the experimental results.[8] As shown in Fig. 3a, there is good agreement, both for the positions and intensities of most peaks, for all of three models and experiment, including the (200), (211), (301), (220), (312), (213), (321) and (325) peaks. Other simulated peaks with $2\theta$ from 45° to 70° are too weak to be used for quantitative analysis.[8] Note that (101) peak is absent in $I2_12_12_1$-$Na_2B_{30}$ and the intensities of

TABLE I. Lattice constants, energy of formation ($\Delta E_f$, with the unit of meV/atom), density ($\rho$), shear modulus (G), bulk modulus (B) and the calculated Vickers hardness ($H_v$) of sodium borides. Some experimental values (from Refs. 7 and 8) are also listed for comparison.

| Parameters | $Na_2B_{30}$ | $Na_2B_{30}$ | $Na_2B_{29}$ | Experiments |
|---|---|---|---|---|
| $Symmetry$ | $I2_12_12_1$ | $Imma$ | $Imm2$ | $Cm^8$, $Imma^7$ |
| $a$ (Å) | 10.42 | 10.29 | 10.34 | $10.40^8$, $10.30^7$ |
| $b$ (Å) | 5.70 | 5.84 | 5.82 | $5.86^8$, $5.85^7$ |
| $c$ (Å) | 8.23 | 8.42 | 8.31 | $8.33^8$, $8.42^7$ |
| $\Delta E_f$ (GGA) | -57.81 | -51.44 | 3.03 | N/A |
| $\Delta E_f$ (LDA) | -63.37 | -45.23 | 13.97 | N/A |
| $\rho$ (g/cm$^{-3}$) | 2.52 | 2.43 | 2.39 | $2.34^8$, $2.44^7$ |
| G (GPa) | 189.02 | 162.50 | 142.03 | N/A |
| B (GPa) | 190.05 | 179.32 | 167.22 | N/A |
| $H_v$ (GPa) | 37.40 | 30.23 | 25.53 | N/A |



FIG. 3. (a) Simulated XRD patterns of the $Imm2$-$Na_2B_{29}$, $Imma$-$Na_2B_{30}$ and $I2_12_12_1$-$Na_2B_{30}$ with the wavelength of 1.54056 Å at ambient pressure compared with the experimental results. (b) Simulated TEM patterns of the $Imm2$-$Na_2B_{29}$, (c) $Imma$-$Na_2B_{30}$, (d) $I2_12_12_1$-$Na_2B_{30}$, (e) experimental result at normal conditions.

(011) and (002) peaks deviate from experimental values to some extent. We speculate that the $I2_12_12_1$-$Na_2B_{30}$ may coexist with $Imma$-$Na_2B_{30}$ (or $Na_2B_{29}$) at ambient conditions. Moreover, the comparison of the measured electron diffraction pattern (TEM) along [010] direction (Fig. 3b) showed that the diffraction spots of all three models again match well with the experimental data.[8] Since the $I2_12_12_1$-$Na_2B_{30}$ structure is very different from $Imma$-$Na_2B_{30}$ or $Imm2$-$Na_2B_{29}$, this example shows that very different structures can have very similar XRD and TEM patterns, making structure determination ambiguous, and in such cases input from theory is invaluable.

Figure 4 shows band structures of $Imma$-$Na_2B_{30}$, $Imm2$-$Na_2B_{29}$, and $I2_12_12_1$-$Na_2B_{30}$ from GGA-PBE calculations. Previously, $Imma$-$Na_2B_{30}$ was thought to be a metal.[11] However, our calculations show that valence and conduction bands exhibit linear dispersion at the Fermi level (Fig. 4a). Further band analysis of $Imma$-$Na_2B_{30}$ indicates that the crossing points form two perpendicular nodal rings (Fig. 4b), which are dominantly originated from the $p$ orbitals of B atoms. Therefore, $Imma$-$Na_2B_{30}$ is a topological nodal line semimetal. The particular nodal rings should be protected by the combination of inversion and time-reversal symmetry,[27] which are expected to have more intensive nonlinear electromagnetic response than Dirac semimetals with a single cone, and thus possess a higher efficiency of carrier trans-
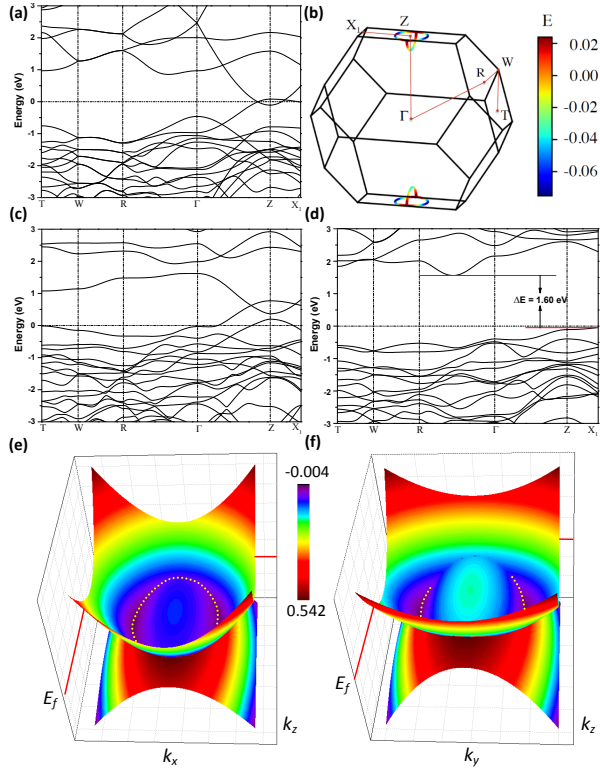
FIG. 4. (a) Band structure of $Imma$-$Na_2B_{30}$ at ambient pressure. (b) Several high-symmetry points in the Brillouin zone of $Imma$-$Na_2B_{30}$ are labelled. The multiple nodal rings center at Z point and the color bar indicates the energy of each nodal point. (c) and (d) show the band structures of $Imm2$-$Na_2B_{29}$ and $I2_12_12_1$-$Na_2B_{30}$ at ambient pressure. (e) and (f) show the band crossings (indicated by yellow dotted lines) of $Imma$-$Na_2B_{30}$ formed by the valence and conduction bands in the vicinity of $Z$ point.



FIG. 5. (a) Phonon DOS of $I2_12_12_1$-$Na_2B_{30}$ and $Imma$-$Na_2B_{30}$ at ambient pressure. (b) The temperature dependence of the free energy for $I2_12_12_1$-$Na_2B_{30}$ and $Imma$-$Na_2B_{30}$ at ambient pressure. The insets show the free energies near 500 and 1000 K.

port at the Fermi level via multiple Dirac channels.[28] In $Imm2$-$Na_2B_{29}$, due to very close structure similarity, the nodal rings could be preserved. However, because of minor concentration of B vacancies, the Fermi level is shifted down by 0.62 eV, to the valence band (Fig. 4c), consequently the hybridized bonding states located at the valence band are partially filled, hence $Imm2$-$Na_2B_{29}$ is metallic. In contrast, $I2_12_12_1$-$Na_2B_{30}$ is an indirect-gap semiconductor with a band gap of 1.6 eV (Fig. 4d). Therefore, as mentioned above, in view of the energetic stability, we see the order of stability $I2_12_12_1$-$Na_2B_{30}$ $>Imma$-$Na_2B_{30}$ $>Imm2$-$Na_2B_{29}$, which is in accordance with the electronic stability among the three compounds, that is, the semiconducting $I2_12_12_1$-$Na_2B_{30}$ $>$semimetallic $Imma$-$Na_2B_{30}$ $>$metallic $Imm2$-$Na_2B_{29}$.

Phonon densities of states (PDOS) of $I2_12_12_1$-$Na_2B_{30}$ and $Imma$-$Na_2B_{30}$ phases are shown in Fig. 5a, both of them are dynamically stable at ambient pressure. In addition, the temperature dependence of the free energy of $I2_12_12_1$-$Na_2B_{30}$ and $Imma$-$Na_2B_{30}$ is shown in Fig. 5b: $I2_12_12_1$-$Na_2B_{30}$ is always more stable than $Imma$-

$Na_2B_{30}$ at least up to the temperature of 1000 K. We also calculated charge distributions of $Imma$-$Na_2B_{30}$ and $I2_12_12_1$-$Na_2B_{30}$. Bader charges show significant difference for the interstitial B atoms: in $Imma$-$Na_2B_{30}$, they are +0.38 and -1.15$e$ for B3 and B5 atoms, whereas they are +0.03 and +0.07$e$ for the interstitial B1 and B8 atoms of the $I2_12_12_1$-$Na_2B_{30}$ structure. More homogeneous Bader charges in the interstitial sublattice correlate with their greater thermodynamic stability at ambient pressure, in agreement with the proposed correlations between local bonding configurations and energetic stability.[29,30] Hence the free energy, electronic stability, formation energy, and charge transfer support that $I2_12_12_1$-$Na_2B_{30}$ is a true thermodynamic ground state, unlike $Imm2$-$Na_2B_{29}$ and $Imma$-$Na_2B_{30}$. Furthermore, boron-rich sodium borides are expected to have superior mechanical properties, e.g., high hardness. According to models,[31,32] Vickers hardness was estimated as $H_v = 0.92k^{1.137}G^{0.708}$ and $k = G/B$, where $G$ and $B$ are shear modulus and bulk modulus. The calculated hardnesses for $Imm2$-$Na_2B_{29}$, $Imma$-$Na_2B_{30}$, and $I2_12_12_1$-$Na_2B_{30}$ (see Table 1) are 25.5, 30.2, and 37.5 GPa, respectively. Thus the semiconducting $I2_12_12_1$-$Na_2B_{30}$ phase is harder than semimetallic $Imma$-$Na_2B_{30}$

or metallic $Imm2$-$Na_2B_{29}$, owing to its special interstitial helical structure, which enhances the energetic stability and hardness.

In conclusion, we performed a systematic search for stable compounds of sodium and boron and identified semiconducting $I2_12_12_1$-$Na_2B_{30}$ as a new ground state structure, which has an unprecedented 3D boron framework with the peculiar interstitial helical structure. Recently, a new silicon allotrope with a quasidirect bandgap was synthesized by using a novel two-step synthesis methodology[33] (consisting of synthesis of $Na_4Si_{24}$ and then removing the Na atoms from the open-framework $Na_4Si_{24}$ structure by the thermal 'degassing' process). Since the channel-like boron host structure is also present in $I2_12_12_1$-$Na_2B_{30}$ (along the $b$-axis), one can attempt to synthesize a new boron allotrope ($I2_12_12_1$-$B_{30}$) by using the same approach.

---

* [xfzhou@nankai.edu.cn](mailto:xfzhou@nankai.edu.cn); [zxf888@163.com](mailto:zxf888@163.com)

[1] J. Nagamatsu, N. Nakagawa, T. Muranaka, Y. Zenitani, and J. Akimitsu, Nature **410**, 63 (2001).

[2] H. Y. Chung, M. B. Weinberger, J. B. Levine, R. W. Cumberland, A. Kavner, J. M. Yang, S. H. Tolbert, and R. B. Kaner, Science **316**, 436 (2007).

[3] R. Mohammadi, A. T. Lech, M. Xie, B. E. Weaver, M. T. Yeung, S. H. Tolbert, and R. B. Kaner, Proc. Natl. Acad. Sci. USA **108**, 10958 (2011).

[4] G. Akopov, M. T. Yeung, and R. B. Kaner, Adv. Mater. **29**, 1604506 (2017).

[5] H. Jang, G. Friemel, J. Ollivier, A. V. Dukhnenko, N. Y. Shitsevalova, V. B. Filipov, B. Keimer D. S. Inosov, Nat. Mater. **13**, 682 (2014).

[6] M. Neupane, N. Alidoust, S.-Y. Xu, T. Kondo, Y. Ishida, D. J. Kim, C. Liu, I. Belopolski, Y. J. Jo, T.-R. Chang, H.-T. Jeng, T. Durakiewicz, L. Balicas, H. Lin, A. Bansil, S. Shin, Z. Fisk, and M. Z. Hasan, Nat. Commun. **4**, 2991 (2013).

[7] R. Naslain, and J. S. Kasper, J. Solid State Chem **1**, 150 (1970).

[8] B. Albert, K. Hofmann, C. Fild, H. Eckert, M. Schleifer, and R. Grurhn, Chem. Eur. J. **6**, 2531 (2000).

[9] B. Albert, Angew. Chem. Int. Ed. **37**, 1117 (1998).

[10] B. Albert, and H. Hillebrecht, Angew. Chem. Int. Ed. **48**, 8640 (2009).

[11] https://www.materialsproject.org/

[12] A. R. Oganov, and C. W. Glass, J. Chem. Phys. **124**, 244704 (2006).

[13] W. Zhang, A. R. Oganov, A. F. Goncharov, Q. Zhu, S. E. Boulfelfel, A. O. Lyakhov, M. Somayazulu, and V. B. Prakapenka, Science **342**, 1502 (2013).

[14] Q. Zhu, D. Y. Jung, A. R. Oganov, C. W. Glass, C. Gatti, and A. O. Lyakhov, Nat. Chem. **5**, 61 (2013).

[15] Y. L. Li, S. N. Wang, A. R. Oganov, H. Gou, J. S. Smith, and T. A. Strobel, Nat. Commun. **6**, 6974 (2015).

[16] X. Dong, A. R. Oganov, A. F. Goncharov, E. Stavrou, S. Lobanov, G. Saleh, G. R. Qian, Q. Zhu, C. Gatti, V. L. Deringer, R. Dronskowski, X. F. Zhou, V. B. Prakapenka, Z. Konôpková, I. A. Popov, A. I. Boldyrev and H. T. Wang, Nat. Chem. **9**, 440 (2017).

[17] P. E. Blöchl, Phys. Rev. B **50**, 17953 (1994).

[18] G. Kresse, and J. Furthmller, Phys. Rev. B **54**, 11169 (1996).

[19] J. P. Perdew, K. Burke, and M. Ernzerhof, Phys. Rev. Lett. **77**, 3865 (1996).

[20] D. M. Ceperley, and B. J. Alder, Phys. Rev. Lett. **45**, 566 (1980).

[21] J. P. Perdew, and A. Zunger, Phys. Rev. B **23**, 5048 (1981).

[22] A. Togo, F. Oba, and I. Tanaka, Phys. Rev. B **78**, 134106 (2008).

[23] R. Hill, Proc. Phys. Soc. London **65**, 350 (1952).

[24] S. J. Clark, M. D. Segall, C. J. Pickard, P. J. Hasnip, M. I. J. Probert, K. Refson, and M. C. Payne, Z. f Krist **220**, 567 (2005).

[25] A. A. Mostofi, J. R. Yates, Y.-S. Lee, I. Souza, D. Vanderbilt, and N. Marzari, Comput. Phys. Commun. **178**, 685 (2008).

[26] Q. S. Wu, S. N. Zhang, H. F. Song, M. Troyera, and A. A. Soluyanov, arXiv:1703.07789.

[27] Q. Xu, R. Yu, Z. Fang, X. Dai, and H. M. Weng, Phys. Rev. B **95**, 045136 (2017).

[28] Y. Jiao, F. Ma, C. Zhang, J. Bell, S. Sanvito, and A. Du, Phys. Rev. Lett. **119**, 016403 (2017).

[29] X. F. Zhou, G. R. Qian, J. Zhou, B. Xu, Y. Tian, and H. T. Wang, Phys. Rev. B **79**, 212102 (2009).

[30] X. F. Zhou, A. R. Oganov, G. R. Qian, and Q. Zhu, Phys. Rev. Lett. **109**, 245503 (2012).

[31] Y. Tian, B. Xu, and Z. Zhao, Int. J. Refract. Met. Hard Mater. **33**, 93 (2012).

[32] X. Q. Chen, H. Niu, D. Li, and Y. Li, Intermetallics **19**, 1275 (2011).

[33] D. Y. Kim, S. Stefanoski, O. O. Kurakevych, and T. A. Strobel, Nat. Mater. **14**, 169 (2015).